Supporting information

Liquid phase exfoliation of bismuth nanosheets for flexible all-solid-state supercapacitors with high energy density

Bingchao Yang,[a] Xiangjun Li,[a] Yong Cheng,[b] Shuai Duan,[a] Bo Zhao,[a] Wencai Yi,[a] Chao Wang,[a] Hairui Sun,[a] Zhixiu Wang,[c] Dapeng Gu,[d] Suwen Chen[e] and Xiaobing Liu*[,a]

[a] *Laboratory of High Pressure Physics and Material Science, School of Physics and Physical Engineering, Qufu Normal University, Qufu 273165, China*

[b] *Department of Materials Science and Engineering, College of Materials, Xiamen University, Xiamen 361005, China*

[c] *Administrative Office of Laboratory and Equipment, Qufu Normal University, Qufu 273165, China*

[d] *School of Mechanical Engineering, Yanshan University, Qinhuangdao 066004, China*

[e] *Department of Environmental and Chemical Engineering, Yanshan University, Qinhuangdao 066004, China.*

***Email**: xiaobing.phy@qfnu.edu.cn

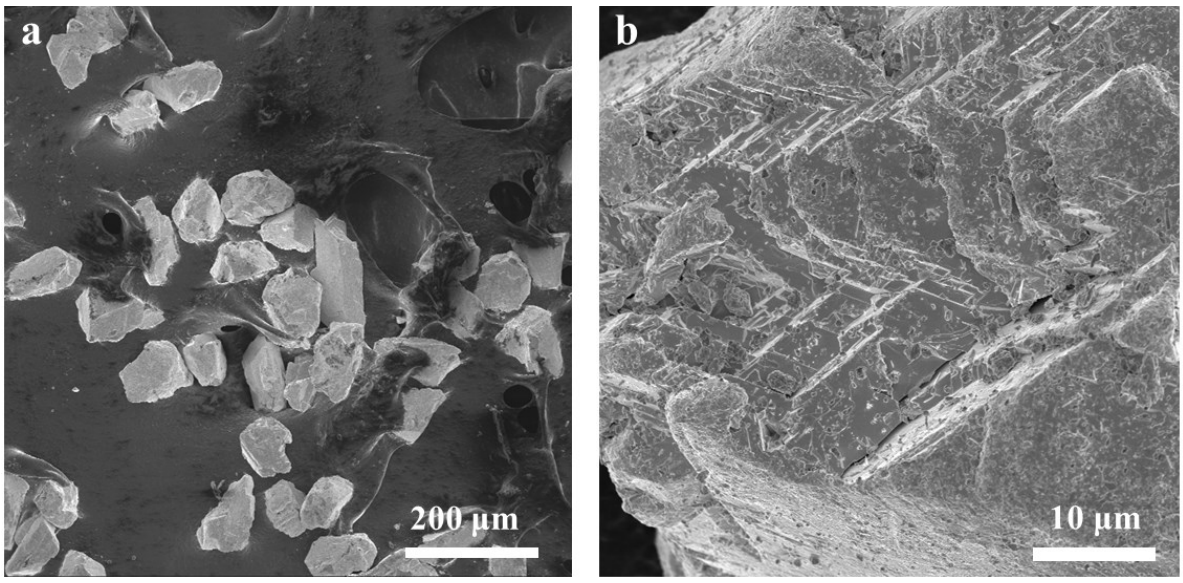

Figure S1. (a, b) Different magnification SEM images of original Bi powders.

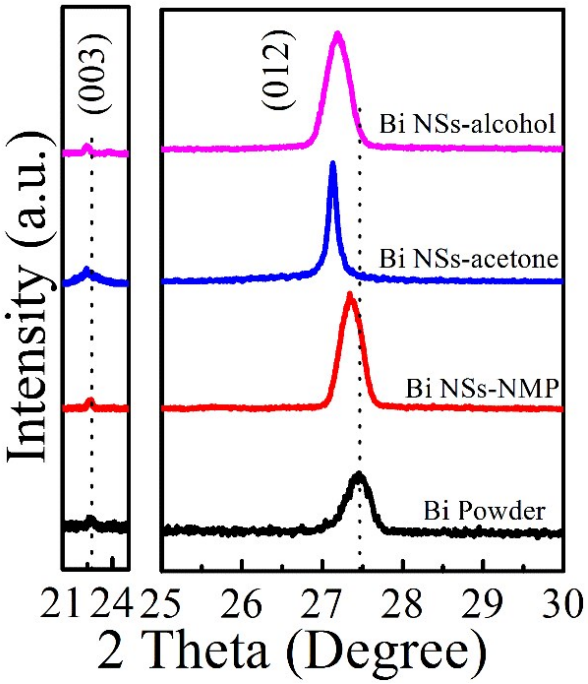

Figure S2. Partial XRD pattern of Bi NSs-alcohol, Bi NSs-acetone, Bi NSs-NMP and Bi powder, (a) (003) peak and (b) (012) peak.

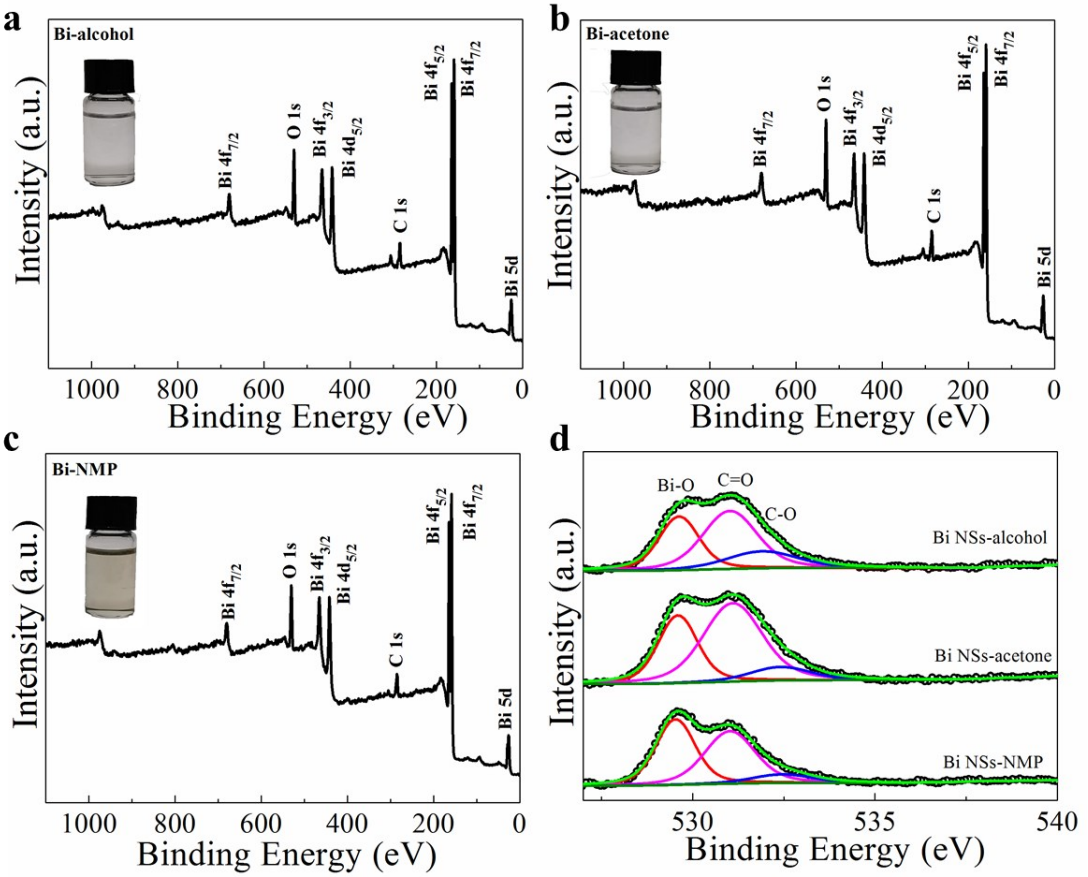

Figure S3. (a-c) XPS survey spectrum and (d) high-resolution O1s spectrum of Bi NSs-alcohol, Bi NSs-acetone and Bi NSs-NMP. Insets: The optical images of 2D Bi nanosheets in alcohol, acetone and NMP solutions.

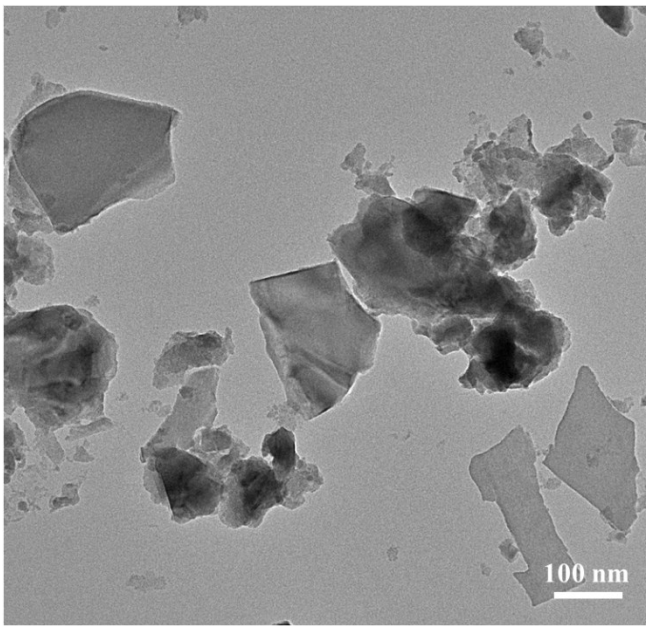

Figure S4. Typical low-magnification TEM image of produced 2D Bi NSs.

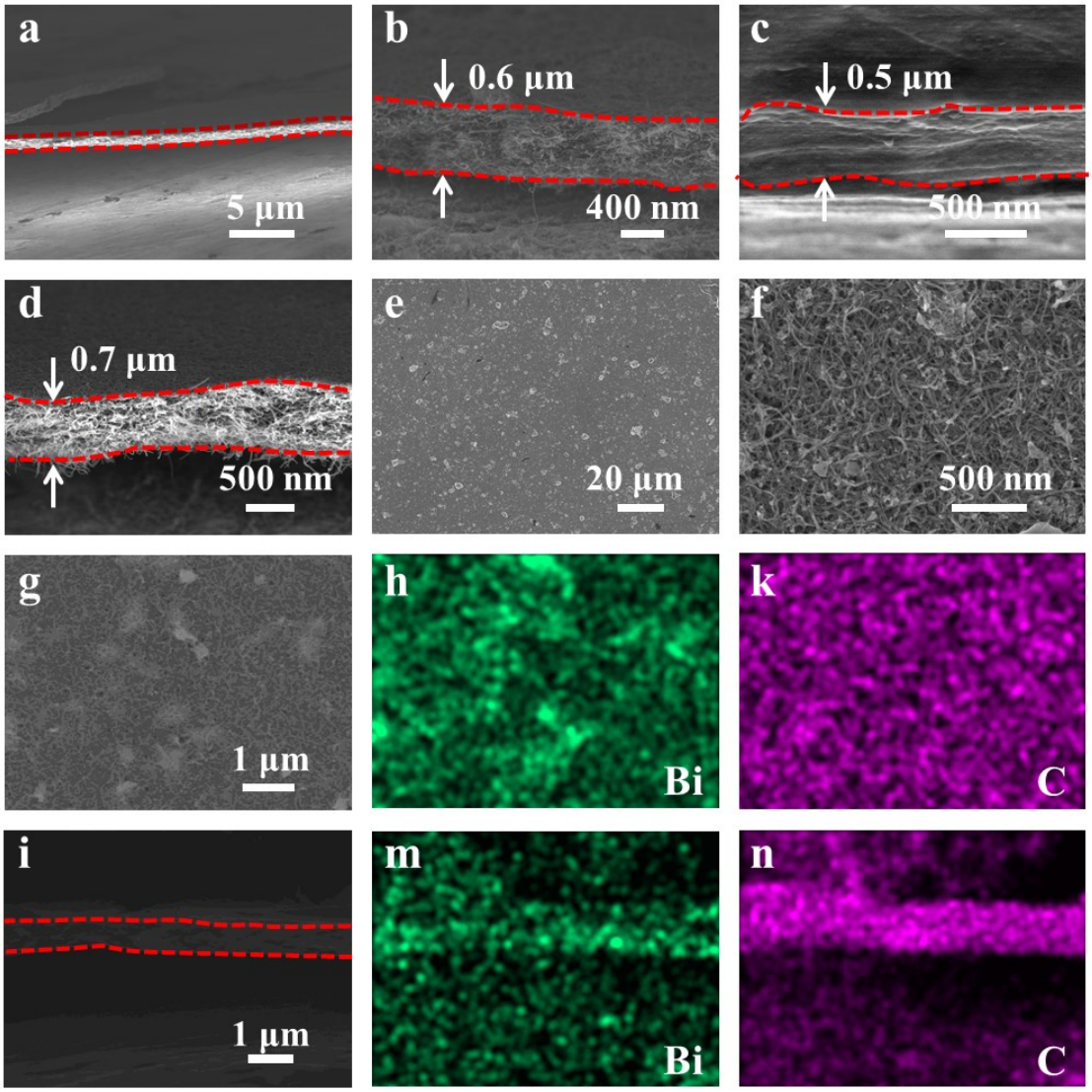

Figure S5. Morphological characterization of Bi/CNTs, Bi and CNTs films. (a) Cross-sectional SEM image of the continuous and uniform Bi/CNTs film. (b-c) Cross-section SEM images for Bi/CNTs, Bi and CNTs films with ~0.6, 0.5 and 0.7 μm in thickness. (e,f) The top view SEM images with different magnification of Bi/CNTs film. (g-k) The SEM image and energy dispersive spectral (EDS) mapping images of Bi-CNTs film. (i-n) Cross-section SEM image of Bi/CNTs film and the corresponding EDS mapping of Bi and C elements.

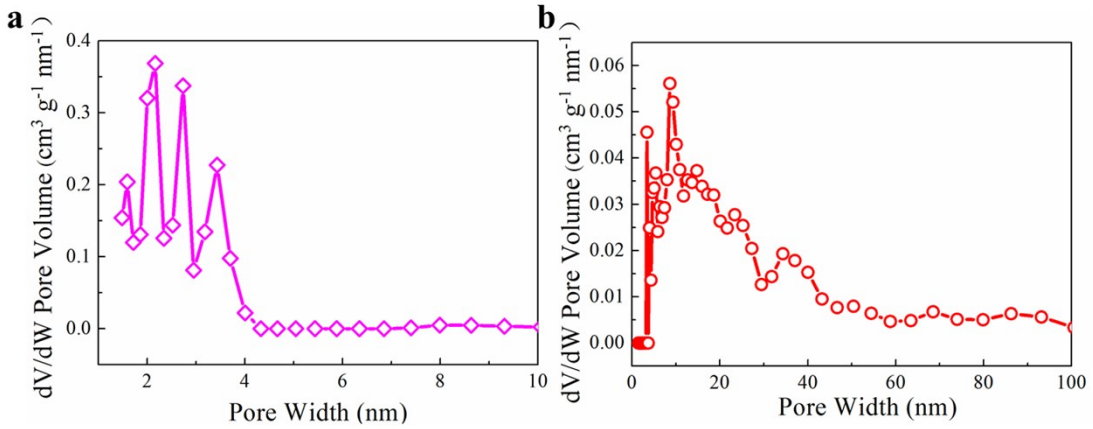

Figure S6. The plot of the pore size distribution of the (a) Bi and (b) Bi/CNTs samples.

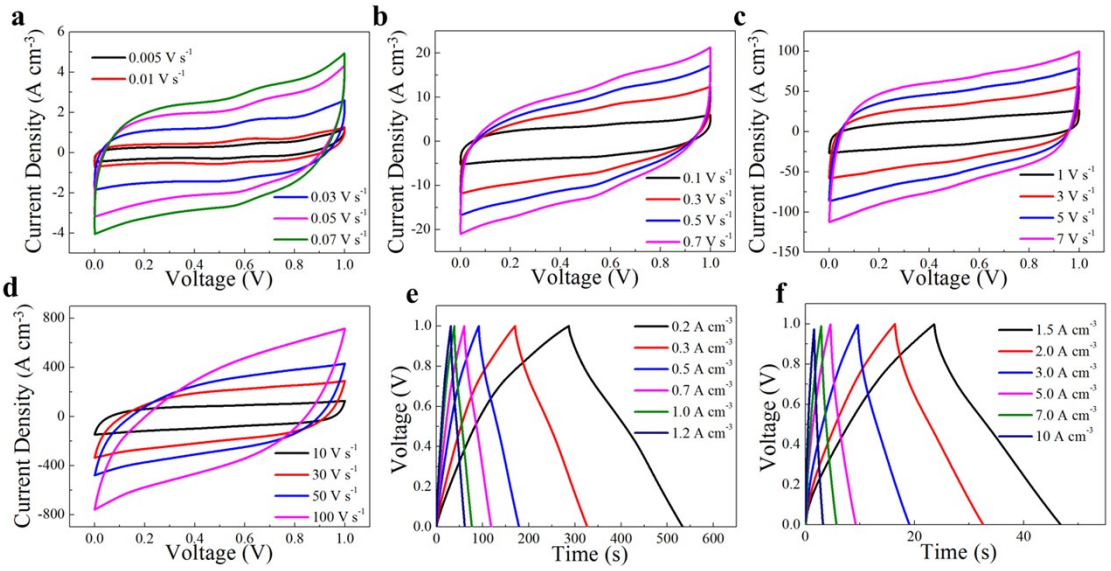

Figure S7. Electrochemical properties of Bi/CNTs ASSP device. (a-d) Cyclic voltammograms at various scan rates from 5 mV s^{-1} to 100 V s^{-1}. (e, f) Galvanostatic charging/discharging curves obtained at different current densities from 0.2 to 10 A cm^{-3}.

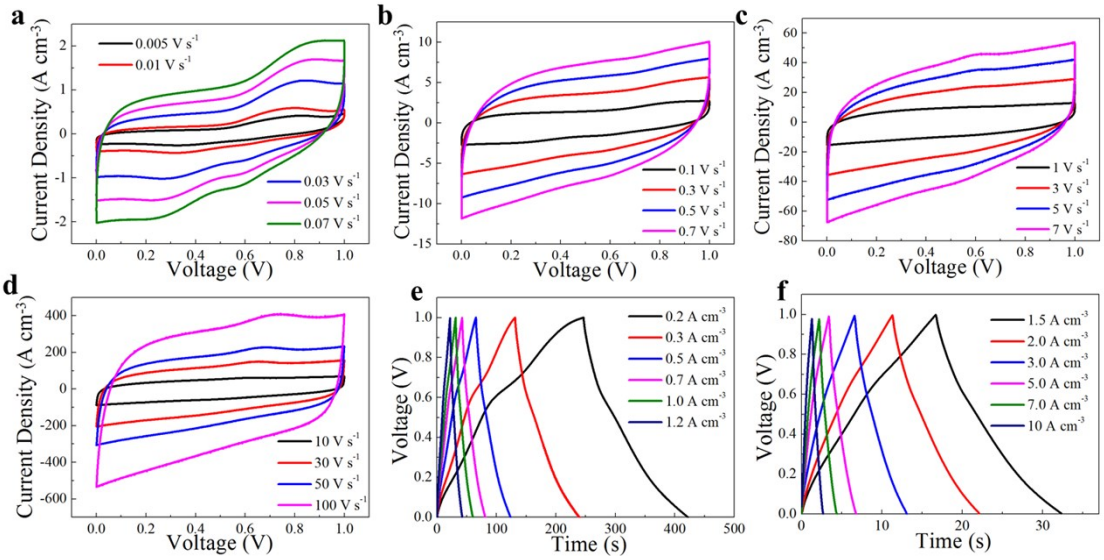

Figure S8. Electrochemical properties of 2D Bi NSs ASSP device. (a-d) Cyclic voltammograms at various scan rates from 5 mV s^{-1} to 100 V s^{-1}. (e, f) Galvanostatic charging/discharging curves obtained at different current densities from 0.2 to 10 A cm^{-3}.

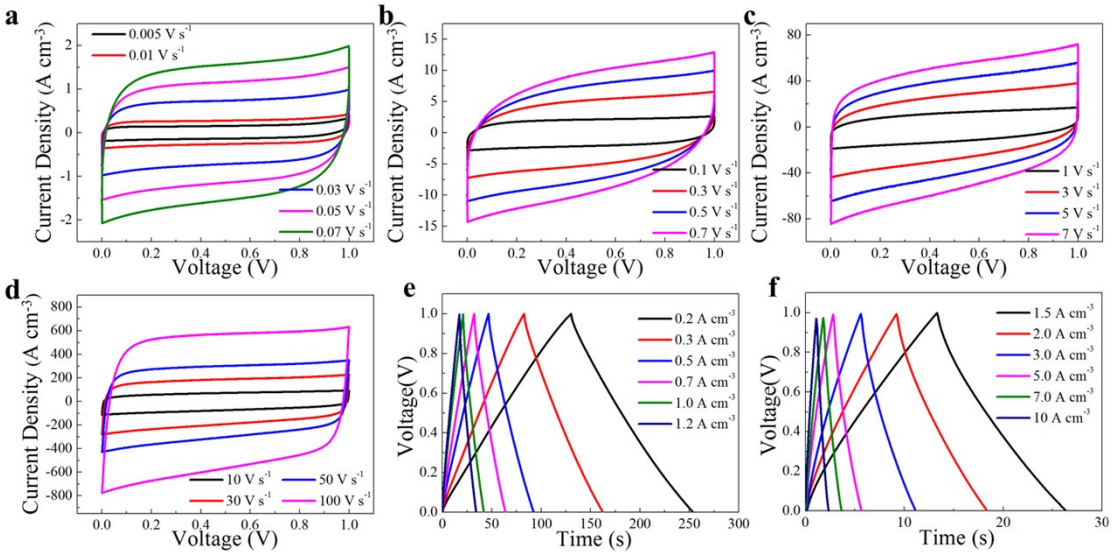

Figure S9. Electrochemical properties of CNTs ASSP device. (a-d) Cyclic voltammograms at various scan rates from 5 mV s^{-1} to 100 V s^{-1}. (e, f) Galvanostatic charging/discharging curves obtained at different current densities from 0.2 to 10 A cm^{-3}.

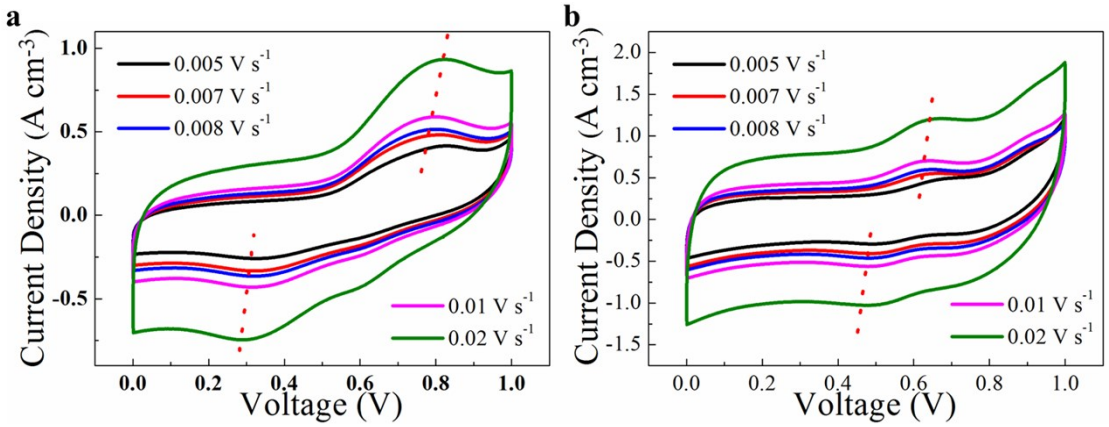

Figure S10. CV curves of (a) Bi and (b) Bi/CNTs ASSP device at scan rates from 5 to 20 mV s^{-1} used for fitting the *b*-values.

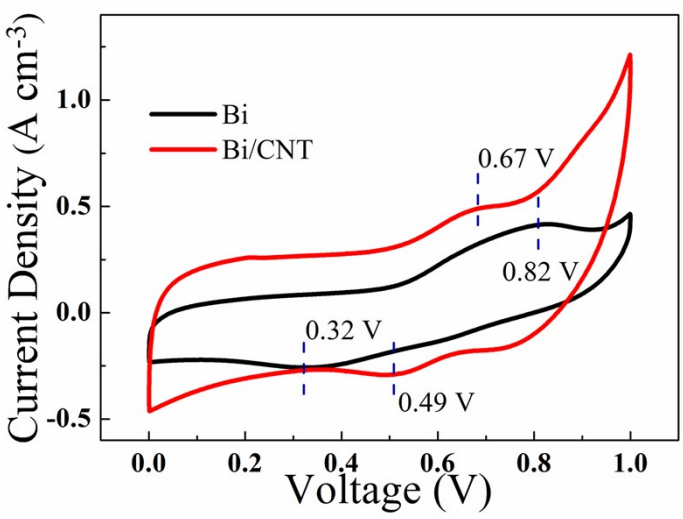

Figure S11. CV curves of Bi and Bi/CNTs ASSP device at can rate of 5 mV s^{-1} in which the redox peaks are located at 0.82/0.32 V and 0.67/0.49 V.

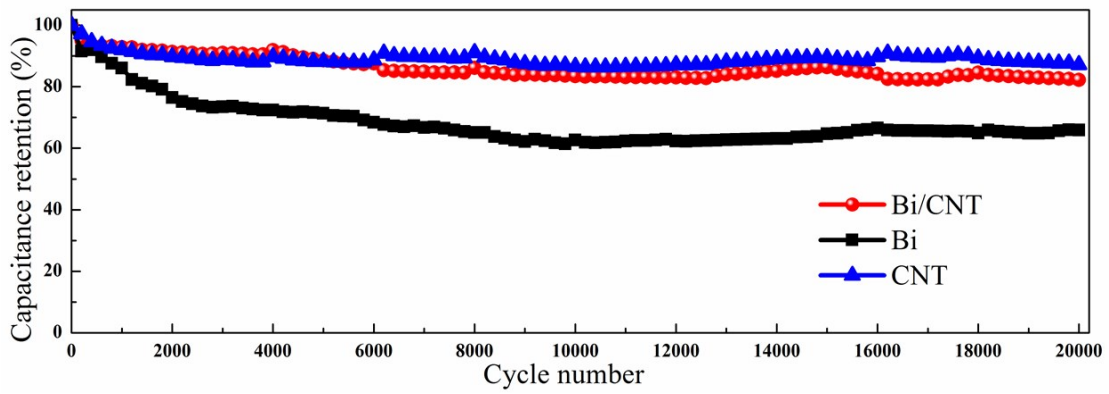

Figure S12. Capacitance retention of Bi/CNTs, Bi and CNTs ASSP device after electrochemical cycling tests of 20,000 cycles at 0.5 V s^{-1}.